The 9th European Congress on Computational Methods in Applied Sciences and Engineering
ECCOMAS Congress 2024
3–7 June 2024, Lisboa, Portugal

MODELING VELOCITY FLUCTUATIONS FOR THE DERIVATION OF AUTOMOTIVE COMPONENT LOADS

Paul Straehle[1,2,*], Steve Wolff-Vorbeck[1], Thomas Leyendecker[1] and Carsten Proppe[2]

[1] Robert Bosch GmbH, Robert-Bosch-Campus 1, 71272 Renningen, Germany

[2] Institute of Engineering Mechanics, Karlsruhe Institute of Technology, 76131 Karlsruhe, Germany

[*] E-Mail: paul.straehle@de.bosch.com

Key words: stochastic modeling, velocity simulation, data analysis, reliability design

Summary. Designing automotive components in a resource-efficient way, it is necessary to know the loads to be expected during operation. At an early stage of development virtual load generation is needed to derive them efficiently and realistically. Many of these loads depend on the driven velocities of the vehicle and, therefore, determining characteristic velocity profiles for different vehicle types and driving manners is essential for reliability-based design in the automotive industry. In the present work we analyse velocity measurements of different vehicles and drivers on several routes and investigate the velocity fluctuations with respect to their statistical properties. We show that the fluctuations can be described by a stochastic process adapted to the measured properties. This leads to a comprehensive stochastic modeling approach that can be used to simulate characteristic velocity profiles for a wide-range of types of roads, drivers and vehicles.

1 Introduction

The established approach to estimate the loads on automotive components is to perform test drives under certain assumptions of the actual usage of the car by a customer. From these assumptions a test route is derived which is then driven in a specific manner by a test driver. The loads measured on this route are then extrapolated to the targeted lifetime of the component. However, due to the high uncertainties associated to the assumptions and the only very limited number of kilometers driven, this approach can only give a limited view into the loads acting on the component over its actual lifetime. In addition, existing physical components (e.g. prototypes or components from previous generations) are required on which the measurements can be carried out. This aspect makes the approach unfeasible for the development of new, innovative components as currently developed for electric and fuel cell electric vehicles. In this case, load measurements must be "virtualized", meaning that they are fully generated by simulations. This requires the modeling of realistic profiles of the speed of the vehicle in driving direction, referred to in the following as the velocity of the vehicle, along an arbitrary route taking into account influences such as traffic and driving behavior.

Present approaches to model velocity profiles show deficiencies related to the random component of velocities, i.e., the fluctuations around a constant mean velocity. In [1], the authors

derive a comprehensive approach where the velocity of the vehicle is modelled using a discrete time series $\{v_{t_i}\}_{i=0}^{N}$ of random variables v_{t_i}. In detail, the velocity is described by

$$v_{t_i} = \bar{v}_{d_{t_i}} X_{t_i} \tag{1}$$

using a mean velocity $\bar{v}_{d_{t_i}}$ at time-dependent position d_{t_i} and the following logarithmic first order Auto-Regressive process (or AR(1) process for short),

$$\begin{aligned} X_{t_i} &= \exp(Z_{t_i} - \frac{\omega^2}{2}), \\ Z_{t_i} &= \eta Z_{t_{i-1}} + \epsilon_{t_i}, \\ \epsilon_{t_i} &\sim \mathcal{N}(0, \sigma_\epsilon). \end{aligned} \tag{2}$$

Here, $\omega^2 = \frac{\sigma_\epsilon^2}{1-\eta^2}$ is a mean correction ensuring that $\mathbb{E}[X_{t_i}] = 1$.

For a given route the mean velocity $\bar{v}_{d_{t_i}}$ is determined by a function depending only on the properties of the road (e.g. traffic lights, speed limit, curvature) at the respective distance

$$d_{t_i} = d_{t_0} + \sum_{j=1}^{i} v_{t_j} \Delta t_j \quad \text{with} \quad \Delta t_j = t_j - t_{j-1}, \tag{3}$$

and on predefined properties of the driver such as tolerated accelerations and adherence to speed limit, see [1] for more details. This means that along an arbitrary route the velocity is described by a deterministic series $\{\bar{v}_{d_{t_i}}\}_{i=0}^{N}$ of mean values and a probabilistic part given by the fluctuation series $\{X_{t_i}\}_{i=0}^{N}$. These fluctuations are the result of internal and external influences, such as inattentiveness of the driver, behaviour of surrounding pedestrians, bikes, cars, etc., which all cause the velocity to contain a stochastic component (e.g. [2]).

Although this approach allows to cover a wide variety of usage scenarios such as the simulation of many different combinations of drivers, cars and routes, it is not sufficient to explain the dynamics of human driving behavior. For example, the evaluation of measured time series of vehicle velocities reveals that the assumption of white noise in (1) is not suitable as in general there is remaining correlation in the residuum ϵ_{t_i}, see Fig. 1. The contribution aims to solve this problem by modeling the vehicle velocity as a dynamical system driven by nonstationary correlated noise (e.g. [3]). Therefore, in Section 2.1 we replace the white-noise in (2) by red-noise, leading to a better reproduction of the measured correlation structure. Furthermore, estimating the statistical properties of the vehicle velocity from various measurements of velocity time series, we find a significant dependence of the fluctuation X_{t_i} on the mean velocity $\bar{v}_{d_{t_i}}$. We, therefore, introduce a coupling of X_{t_i} and $\bar{v}_{d_{t_i}}$ in Section 2.2 developing a novel approach for the modeling of human driving behavior.

In Section 3, we demonstrate the improved properties of the approach, developed in Section 2, for the generation of virtual loads. To do so, we evaluate simulated velocity profiles in comparison to measured velocities and show decisive advantages of the approach in a damage modeling use-case for automotive components.

2 Modeling of velocity fluctuations

2.1 Stochastic process identification

To derive a comprehensive modelling approach for the simulation of vehicle velocity we extend the approach described by (1) and consider the following time series $\{v_{t_i}\}_{i=0}^{N}$ of vehicle velocities defined by:

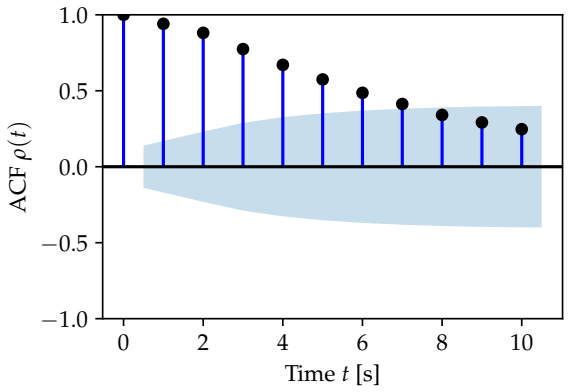

Figure 1: Auto-correlation of residuum ϵ_{t_i} with a white-noise AR(1) processes for a window

$$v_{t_i} = \bar{v}_{d_{t_i}} X_{t_i} \tag{4}$$

with

$$\begin{aligned} X_{t_i} &= \exp(Z_{t_i} - \frac{\omega^2}{2}), \\ Z_{t_i} &= \eta Z_{t_{i-1}} + \epsilon_{t_i}, \\ \epsilon_{t_i} &\sim \mathcal{N}(0, \sigma_\epsilon) \end{aligned} \tag{5}$$

for $\eta \in (0, 1)$ where the noise term ϵ_{t_i} is itself an AR1-process, i.e.,

$$\begin{aligned} \epsilon_{t_i} &= \theta \epsilon_{t_{i-1}} + \zeta_{t_i}, \\ \zeta_{t_i} &\sim \mathcal{N}(0, \sigma_\zeta) \end{aligned} \tag{6}$$

for $\theta \in (0, 1)$. Here the mean correction is adapted to the additional correlation in the noise

$$\omega^2 = \left(\frac{1 + \eta\theta}{1 - \eta\theta}\right)\left(\frac{\sigma_\zeta^2}{(1 - \eta^2)(1 - \theta^2)}\right) \tag{7}$$

such that $\mathbb{E}[X_{t_i}] = 1$.

2.2 Parameter estimation

For the estimation of the parameters η, θ and σ_ζ we use available measurements of vehicle velocities as, for instance, depicted in Fig. 2a. To consider the influence of the parameters η, θ and σ_ζ on the vehicle velocity the series is split into short windows of length $t_{wl} = 200\,\mathrm{s}$, see Fig. 2b. For each window we compute the mean velocity $\bar{v}$ and normalise the velocity in the respective window with respect to $\bar{v}$. For each window the parameters are then estimated following the approach in [3, Section 3] using an unbiased estimator for the parameters θ, η and σ_ζ. We mention that the procedure depicted in [3, Section 3] is based on the unbiased estimators for η and θ derived in [4, 5].

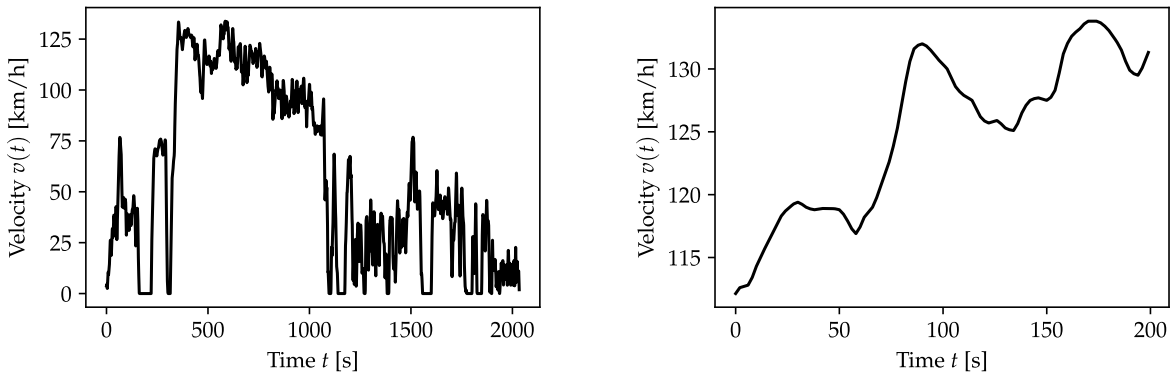

(a) Velocity series of a trip

(b) Velocity series of a window

Figure 2: Example of velocity series

The same analysis is now performed on multiple windows taken from multiple trips over a wide variety of roads with a single driver where for each window i the tuple $\boldsymbol{p}_i = (\eta_i, \zeta_i, \sigma_{\zeta,i})$ as well as the minima and maxima of the window $\underline{z}_i, \bar{z}_i$ are estimated. This way we obtain two families of parameters $(\boldsymbol{p}_i)_i = (\eta_i, \zeta_i, \sigma_{\zeta,i})_i$ and $(\boldsymbol{z}_i)_i = (\underline{z}_i, \bar{z}_i)_i$ representing the combination of parameters and the minima/maxima for each window. The parameter estimates $(\boldsymbol{p}_i)_i$ of each window are then binned according to the mean velocity $(\bar{v}_i)_i$ of the window leading to a multivariate distribution of the parameters $(\boldsymbol{p}_i)_i = (\eta_i, \zeta_i, \sigma_{\zeta,i})_i$ for each velocity bin. The distribution for each bin is then described by a multivariate normal distribution

$$f_{\boldsymbol{P}|\bar{v}}(\boldsymbol{p}|\bar{v}) \sim \mathcal{N}(\boldsymbol{\mu}, \boldsymbol{\Sigma}) \tag{8}$$

where the vector of mean values $\boldsymbol{\mu}$ and the covariance matrix $\boldsymbol{\Sigma}$ are estimated from the available parameter values $(\boldsymbol{p}_i)_i$ within the respective bin. Here, for each $\boldsymbol{p}_i$ in the bin we consider the logarithm $\log(\sigma_{\zeta,i})$ of the standard deviation instead of the standard deviation itself such that the conditional distribution of $\sigma_{\zeta,i}$ with all other parameters fixed will be given by a one-dimensional lognormal distribution. In Fig. 3, this procedure is illustrated for the velocity bin including the mean velocities $100\,\mathrm{km/h} < \bar{v}_i < 110\,\mathrm{km/h}$, where the measured parameter tuples $(\boldsymbol{p}_i)_i$ for the bin and the projected 1, 2 and 3-sigma ellipses of the fitted normal distribution are depicted.

As for the parameters $(\boldsymbol{p}_i)_i$ the minima $(\underline{z}_i)_i$ and maxima $(\bar{z}_i)_i$ of each window are binned according to the mean velocities $(\bar{v}_i)_i$ of the windows. From the resulting histograms per bin of the maxima and minima the 99%-quantile $q_{0.99}(\bar{z}_i)$ for $(\bar{z}_i)_i$ and the 1%-quantile for $(\underline{z}_i)_i$ are determined. These quantiles are used in the further course of the work to adapt proper bounds to the velocity fluctuation X_{t_i}, see the following Section 2.3. Taking quantiles of the minima and maxima the estimation of the bounds will be less sensitive to outliers. In Fig. 3b the histogram of the upper limits $\bar{z}_i$ and the corresponding 99%-quantile for the mean velocity range $100\,\mathrm{km/h} < \bar{v}_i < 110\,\mathrm{km/h}$ is depicted.

The estimation of the multivariate normal distribution for the parameters η, θ and $\log(\sigma_\zeta)$ and the derivation of the lower $q_{0.01}(\underline{z}_i)$ and upper quantiles $q_{0.99}(\bar{z}_i)$ is repeated for all velocity bins.

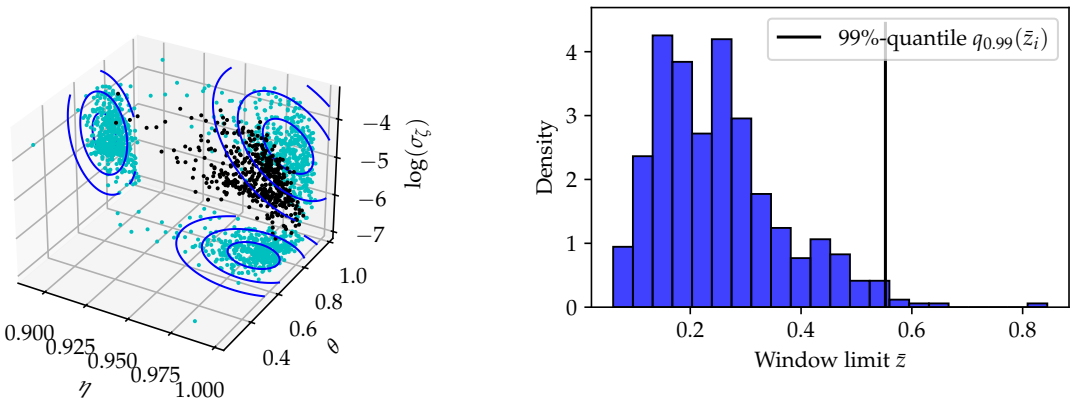

(a) Measured parameter tuples $\boldsymbol{p}_i$ and fitted multivariate normal distribution

(b) Histogram of upper limits $\bar{z}_i$ and the corresponding 99%-quantile

Figure 3: Distribution of $\boldsymbol{p}_i$ and $\bar{z}_i$ for mean velocity bin $100\,\mathrm{km/h} < \bar{v}_i < 110\,\mathrm{km/h}$

Using continuous interpolation of the parameters $\boldsymbol{\mu}, \boldsymbol{\Sigma}$ and the bounds $q_{0.01}(\bar{z}_i)$ and $q_{0.99}(\bar{z}_i)$ along the velocity bins they can be described as a continuous function of the mean velocity $\bar{v}$.

As mentioned in the introduction a significant trend of each parameter with respect to the mean velocity can be observed. The mean of the correlation parameters μ_η and μ_θ, for instance, increases with rising mean velocity indicating less random velocity fluctuations which in our case corresponds to less random and smoother driving behaviour, see Fig. 4a and 4b. This is sensible as on trips in urban areas random events are usually less predictable and on short term notice due to the higher interaction with other road users and the worse long distance visibility. On motorways the velocities show higher correlations, i.e., are smoothed out as the random events there are usually more predictable, such as cars braking in the distance or upcoming lane changes and the generally better long distance visibility.

On the other hand the mean of the logarithmic standard deviation $\mu_{\log(\sigma_\zeta)}$ decreases when the mean velocity increases, indicating a decreasing amplitude of the velocity fluctuations with increasing velocity in line with the expectation of a smoother driving behaviour at higher velocities on motorways and vice versa, see Fig. 4c.

2.3 Bounded time-discrete processes

In general, as the AR(1) process in equations (4) and (5) is normally distributed, the logarithmic red-noise AR(1) process as described in Section 2.1 follows a log-normal distribution. The log-normal distribution is supported on $X_{t_i} \in (0, \infty)$, i.e., velocities can theoretically reach any value in the range from 0 to ∞. This is not only a theoretical problem with a probability close to zero but can actually lead to unrealistic velocities in practical applications as depicted in Fig. 5a, which shows 100 samples created around a mean velocity of $\bar{v} = 80\,\mathrm{km/h}$ with typical values for η, θ and σ_ζ. The frequent velocity peaks of up to 140 km/h never occur in the velocity measurements used to parameterize the stochastic process in this example. Therefore, it is necessary to bound the process in (4) to realistic velocities that are consistent with the velocities obtained from measurements. To bound the process according to measured vehicle velocities we

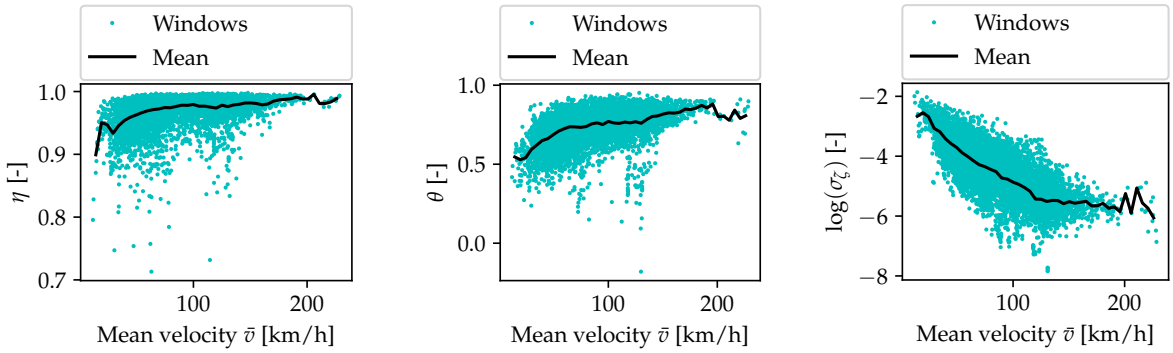

(a) μ_η (b) μ_θ (c) $\mu_{\log(\sigma_\zeta)}$

Figure 4: Relationship between $\mu_\eta, \mu_\theta, \mu_{\log(\sigma_\zeta)}$ and mean velocity $\bar{v}$

use the bounds $\underline{z} = q_{0.01}(\underline{z}_i)$ and $\bar{z} = q_{0.99}(\bar{z}_i)$ on Z_{t_i} derived in Section 2.2.

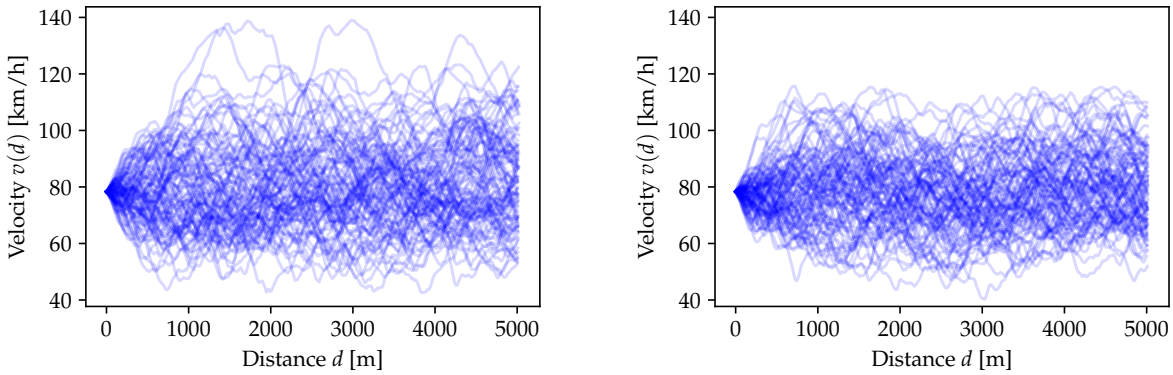

(a) Not bounded (b) Bounded

Figure 5: 100 samples of velocity fluctuations generated with a bounded and not bounded red-noise AR(1) process

In [6] the authors derive an approach for a bounded AR process. This approach is based on a truncation of the noise term ζ to ensure that the process Z_{t_i} is bounded by a lower limit $\underline{z}$ and upper limit $\bar{z}$ and leads to a sharp bound on the distribution of Z_{t_i}. An alternative is to truncate the process by resampling until a feasible solution is found. In practice this could lead to undesired run-times when the probability of achieving a feasible solution is low. By decreasing the standard deviation σ_ζ at each resampling iteration until zero a solution within a specific number of iterations n_{max} can be guaranteed. In the implemented solution σ_ζ is reduced in each iteration r_p using the function

$$\sigma_{\zeta,r_p} = \sigma_{\zeta,0}\left(1 - \frac{r_p}{n_{max}}\right)^a \tag{9}$$

where in the following applications we set $a = 10$ and $n_{max} = 100$. This leads to an almost unchanged standard deviation σ_{ζ,r_p} for the first approx. 60 iterations during which in most cases a feasible solution is found. After 60 iterations an increasingly steep decline of the standard deviation begins, guaranteeing a feasible solution within a maximum of 100 iterations.

Resulting from the resampling algorithm is a distribution of the stochastic process Z_{t_i} which is bounded by $\underline{z}$ and $\bar{z}$, where the distribution is not cut off at the bounds but is gradually tapered towards its limits. The gradual tapering is desired for the modeling of velocity fluctuations, as there are no sharp lower or upper bounds to the velocity fluctuations in reality which would lead to an unrealistic accumulation of velocities near the bounds.

2.4 Simulation of velocity profiles

To simulate the velocity of the vehicle along an arbitrary route we use a one-dimensional discretization $\{d_k\}_{k=0}^{M}$ of the route distance such that two points d_k and d_{k+1} represent a route section $[d_k, d_{k+1})$. We specify the series of mean velocities $\{\bar{v}_k\}_{k=0}^{M}$ on each route section as the minimum between the actual speed limit v_l^k and the traffic-related maximum speed v_{max}^k at the center point $\bar{d}_k = (d_k + d_{k+1})/2$. Both the speed limit v_l^k and the maximum speed v_{max}^k are inferred from available route data by matching the center point $\bar{d}_k$ to its corresponding latitude and longitude coordinates on an existing map. In this framework stop events can be included setting the speed limit $v_k^l = 0$ at specific positions. To generate a time-dependent velocity series v_{t_i} the parameters η, θ and σ_ζ are determined by drawing samples from the conditional normal distribution $f_{\boldsymbol{P}|\bar{V}}(\boldsymbol{p}|\bar{v})$ for each route section considering the mean velocity $\bar{v}_k$ at $\bar{d}_k$. Moreover, for every route section the lower and upper limits $q_{0.01}(\underline{z}_i)$ and $q_{0.99}(\bar{z}_i)$ are specified according to Section 2.2.

On every route section a time-dependent velocity series $\{v_{t_i}\}_{i=0}^{N}$ is generated using equations (4) and (5) where the parameters η, θ and σ_ζ are fixed on each section. Here, we set the initial conditions $Z_0 = 0$ and $\epsilon_0 = 0$ for the first route section $[d_0, d_1)$ where for the remaining sections the initial values are inferred from the respective values at the end of the previous section. For every route section the resampling is executed according to Section 2.3 ensuring that the velocity lies within the bounds $q_{0.01}(\underline{z}_i)$ and $q_{0.99}(\bar{z}_i)$. The red-noise AR(1) process in equations (4) and (5) is executed with a constant time step of $\Delta t_i = 1\,\mathrm{s}$ which results in a distance of $\Delta d_{t_i} = v_{t_i}\Delta t_i$ driven in each iteration. Finally, the resulting series of velocities $\{v_{t_i}\}_{i=0}^{M(N+1)-1}$ along the route is filtered using Gaussian kernel smoothing resulting in a continuously differentiable and instantionary stochastic process describing the vehicle velocity along the route, see Fig. 6b.

3 Evaluation of the model

In Fig. 6a we illustrate the simulated velocity series using both the model described in [1], see equation (1), and the method developed in this contribution, see equations (4) and (5). Moreover, the measured velocity for the respective route section is depicted revealing that the approach in (4)and (5) can reproduce the correlation structure of the measured velocity much better. In Fig. 6b we compare the simulated velocity series for a full motorway trip of length $\sim 80\,\mathrm{km}$ with a respective measurement, displaying a good replication of the measurement due to the realistic and constantly changing mean, variance and correlation properties of the simulated velocity series.

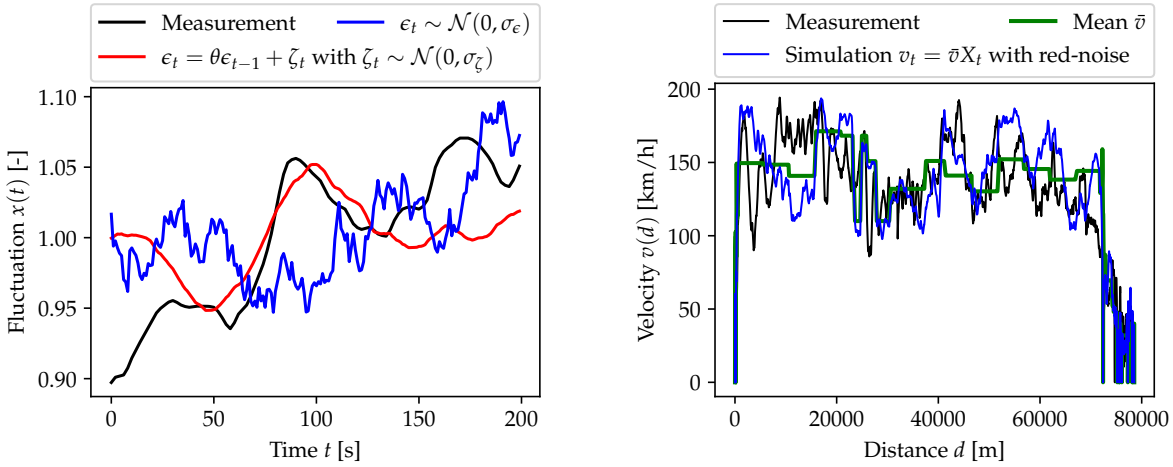

(a) Samples of logarithmic AR(1) processes with white- and red-noise compared to measurement

(b) Comparison of simulated (with red-noise) and measured velocity series for a motorway trip

Figure 6: Comparison of velocity simulation results for a window and a full trip

Moreover, as an important property of the velocity series relevant for load generation we consider the number and amplitude of rainflow cycles included in the series, see, for instance, [7]. To evaluate the rainflow cycles of the velocity series, we simulate multiple routes driven by the same driver using the procedure described in Section 2.4 and compare the rainflow histogram for measured and simulated velocities, see Fig. 7. Comparing the rainflow histograms indicates that the consideration of correlation in the noise term ϵ_{t_i} in (5) and the coupling of $\bar{v}_{d_{t_i}}$ and X_{t_i} in (4) leads to velocity profiles that well reproduce the number and amplitude of rainflow cycles compared to measured velocities. When using the white-noise approach a distinct overestimation of the number of small velocity cycles becomes visible, a result of the lack of correlation in the noise term leading to more small fluctuations as visible in Fig. 6a.

Further we depict an exemplary use-case of load generation using simulated velocities. In the following example the torque load in the drive-train is estimated with a simple system simulation model calculating the forces acting on the vehicle from the respective velocity simulated with the model described above, see [8]. This way a time series of the torque acting on drive-train components of the vehicle is derived. From the torque series the gear damage sum D_G, as it could be used in gear dimensioning according to ISO 6336-6 [9], is calculated. Here, D_G is calculated for windows of length $s_{wl} = 5000\,\mathrm{m}$ and with a shift of $s_{ws} = 500\,\mathrm{m}$. As we are only interested in illustrating the influence of load generation on the damage sum D_G without considering a particular component and its properties, the damage sum per window $D_{G,i}$ is normalised to the length of the window i and the maximum damage sum per window $D_{G,max}$ leading to the normalised damage per window defined by

$$D'_{G,i} = \frac{D_{G,i}}{s_{wl} D_{G,max}}. \tag{10}$$

The distribution of the damage sum $D'_{G,i}$ over all windows is depicted in Fig. 8 and shows a good agreement between the damage sums derived from measured loads and those derived from

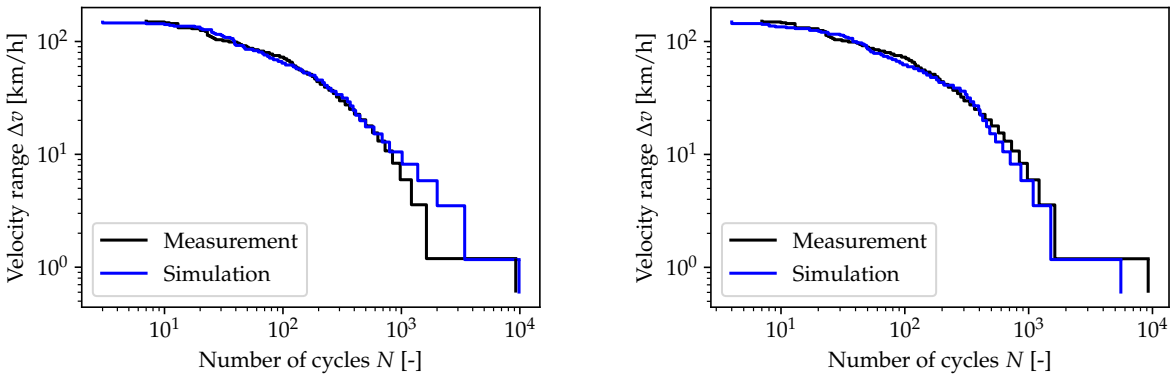

(a) White-noise

(b) Red-noise

Figure 7: Comparison of velocity rainflow histogramms for multiple routes of the same driver

simulated loads using the red-noise approach. With white-noise the number of windows with small damage sums is underestimated, a result of the overestimation of the number of small velocity cycles due to the lack in the correlation of the noise in the velocity series, see Fig. 7a.

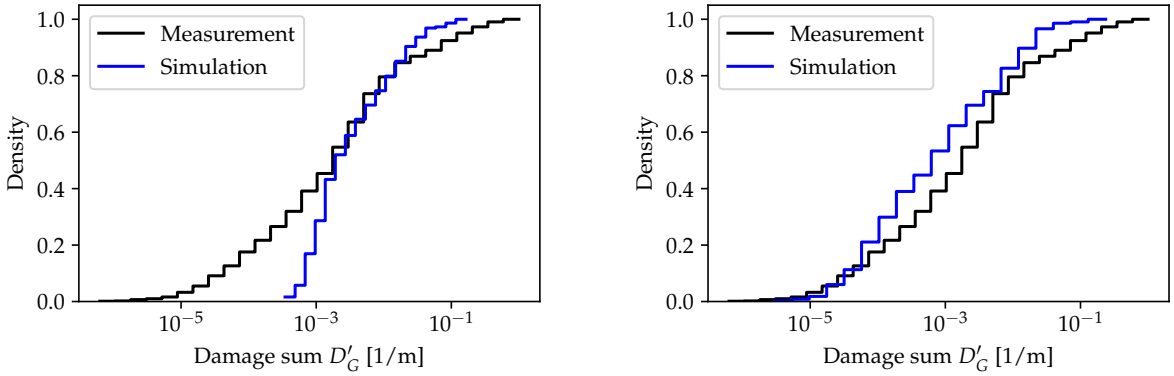

(a) White-noise

(b) Red-noise

Figure 8: Distribution of gear damage sum $D'_{G,i}$ per window derived from simulated and measured torque load for multiple routes of the same driver

4 Conclusion

In the first part of this contribution we presented an improvement to the stochastic process used to model velocity fluctuations within the velocity simulation framework described in [1]. The new approach is based on a red-noise AR(1) process which allows for a better representation of the correlation structure observed in measured velocities, see Fig. 6a. A method to bound the stochastic process is developed to ensure that the produced velocity fluctuations remain within a realistic range. Moreover, the extended stochastic process is coupled with a novel

approach to model its parameters. The distribution and dependence of the parameters for a certain mean velocity are described by a multivariate normal distribution. In order to model the change in velocity fluctuations, e.g., to differentiate between city and motorway driving, the mean vector and covariance matrix of the distribution depend on the mean velocity. Results show that the new stochastic process and its parameterization produce realistic velocity series. This is demonstrated by the close match of the rainflow histogram for measured and simulated velocities for multiple routes, see Fig. 7b. Moreover, we illustrated the ability of the new model to generate realistic loads on vehicle components using simulated velocities. This is demonstrated in a use-case example showing a close match of the gear damage sums between simulated and measured loads, see Fig. 8b.

References

[1] K. Sandmann, T. Leyendecker, M. Burger, and M. Speckert. *Ableitung von feldrelevanten Lastkollektiven mittels Stochastischer Verkehrssimulation*. 2018. URL: https://publica.fraunhofer.de/handle/publica/403187.

[2] Zhen-Hua Li, Shi-Teng Zheng, Rui Jiang, Jun-Fang Tian, Kai-Xuan Zhu, and Roberta Di Pace. "Empirical and simulation study on traffic oscillation characteristic using floating car data". In: *Physica A: Statistical Mechanics and its Applications* 605 (Nov. 2022), p. 127973. ISSN: 03784371. DOI: 10.1016/j.physa.2022.127973. URL: https://linkinghub.elsevier.com/retrieve/pii/S0378437122006136 (visited on 11/30/2023).

[3] Christopher Boettner and Niklas Boers. "Critical slowing down in dynamical systems driven by nonstationary correlated noise". In: *Physical Review Research* 4.1 (Mar. 28, 2022), p. 013230. ISSN: 2643-1564. DOI: 10.1103/PhysRevResearch.4.013230. URL: https://link.aps.org/doi/10.1103/PhysRevResearch.4.013230 (visited on 12/05/2023).

[4] Bernard Bercu and Frédéric Proïa. "A sharp analysis on the asymptotic behavior of the Durbin–Watson statistic for the first-order autoregressive process". In: *ESAIM: Probability and Statistics* 17 (2013), pp. 500–530.

[5] Edmond Malinvaud. "Estimation et prévision dans les modeles économiques autorégressifs". In: *Revue de l'Institut international de statistique* (1961), pp. 1–32.

[6] Josep Lluís Carrion-i-Silvestre, María Dolores Gadea, and Antonio Montañés. "Nearly Unbiased Estimation of Autoregressive Models for Bounded Near-Integrated Stochastic Processes*". In: *Oxford Bulletin of Economics and Statistics* 83.1 (Feb. 2021), pp. 273–297. ISSN: 0305-9049, 1468-0084. DOI: 10.1111/obes.12399. URL: https://onlinelibrary.wiley.com/doi/10.1111/obes.12399 (visited on 12/20/2023).

[7] C Amzallag, J Gerey, J Robert, and J Bahuaud. "Standardization of the rainflow counting method for fatigue analysis". In: *International Journal of Fatigue* 16.4 (June 1994), pp. 287–293. ISSN: 01421123. DOI: 10.1016/0142-1123(94)90343-3. URL: https://linkinghub.elsevier.com/retrieve/pii/0142112394903433 (visited on 12/05/2023).

[8] Hans-Hermann Braess and Ulrich Seiffert, eds. *Vieweg Handbuch Kraftfahrzeugtechnik*. Wiesbaden: Springer Fachmedien Wiesbaden, 2013. ISBN: 978-3-658-01690-6 978-3-658-01691-3. DOI: 10.1007/978-3-658-01691-3. URL: http://link.springer.com/10.1007/978-3-658-01691-3 (visited on 06/13/2024).

[9] ISO 6336-6. *Calculation of load capacity of spur and helical gears — Part 6: Calculation of service life under variable load*. Version Second edition 2019-11. Geneva, 2019.